

MultiGrain: a unified image embedding for classes and instances

Maxim Berman* Hervé Jégou Andrea Vedaldi Iasonas Kokkinos Matthijs Douze
 ESAT-PSI, KU Leuven Facebook AI Research

Abstract

MultiGrain is a network architecture producing compact vector representations that are suited both for image classification and particular object retrieval. It builds on a standard classification trunk. The top of the network produces an embedding containing coarse and fine-grained information, so that images can be recognized based on the object class, particular object, or if they are distorted copies. Our joint training is simple: we minimize a cross-entropy loss for classification and a ranking loss that determines if two images are identical up to data augmentation, with no need for additional labels. A key component of MultiGrain is a pooling layer that allow us to take advantage of high-resolution images with a network trained at a lower resolution.

When fed to a linear classifier, the learned embeddings provide state-of-the-art classification accuracy. For instance, we obtain 79.3% top-1 accuracy with a ResNet-50 learned on Imagenet, which is a +1.7% absolute improvement over the AutoAugment method. When compared with the cosine similarity, the same embeddings perform on par with the state-of-the-art for image retrieval at moderate resolutions.

1. Introduction

Image recognition is central to computer vision, with dozens of new approaches being proposed every year, each optimized for particular aspects of the problem. From coarse to fine, we may distinguish the recognition of (a) classes, where one looks for a certain type of object regardless of intra-class variations, (b) instances, where one looks for a particular object despite changes in the viewing conditions, and (c) copies, where one looks for a copy of a specific image despite edits. While these problems are in many ways similar, the standard practice is to use specialized, and thus incompatible, image representations for each case.

Specialized representations may be accurate, but constitute a significant bottleneck in some applications. Consider for example image retrieval, where the goal is to match a query image to a large database of other images. Very often



Figure 1: Our goal is to extract an image descriptor incorporating different levels of granularity, so that we can solve, in particular, classification and particular object recognition tasks: The descriptor is either fed to a linear classifier, or directly compared with cosine similarity.

one would like to search the same database with multiple granularities, by matching the query by class, instance, or copy. The performance of an image retrieval system depends primarily on the *image descriptors* it uses. These strike a trade-off between database size, matching and indexing speed, and retrieval accuracy. Adopting multiple descriptors, narrowly optimized for each type of query, means multiplying the size of the database, which is often unacceptable.

In this paper we present a new representation, MultiGrain, that can achieve the three tasks together, regardless of differences in their semantic granularity, see fig. 1. We learn MultiGrain by jointly training an image embedding for multiple tasks. The resulting representation is compact and outperforms narrowly-trained descriptors.

Instance retrieval has a wide range of industrial applications, including detection of copyrighted images, or exemplar-based recognition of unseen objects. In settings where billion images have to be treated, it becomes of interest to obtain image embeddings suitable for more than one recognition task. For instance, an image storage platform is likely to perform some classification of the input images, aside from detecting copies or instances of the same object. An embedding relevant to all these tasks advantageously reduces both the computing time per image and storage space.

*Did this work during an internship at Facebook AI Research.

In this perspective, convolutional neural networks trained only for classification already go a long way towards universal features extractors [37]. The fact that we can learn image descriptors that are simultaneously good for classification and instance retrieval is surprising but not contradictory. In fact, there is a logical dependence between the tasks: images that contain the same instance also contain, by definition, the same class; and copied images contain the same instance. This is in contrast to multi-task settings where tasks are in competition and are thus difficult to combine [29, 49]. Instead, both class, instance, and copy congruency lead to descriptors that should be close in feature space. Still, the degree of similarity is different in the different cases, with classification requiring more invariance to appearance variations and copy detection sensitivity to small image details.

In order to learn an image representation that satisfies the different trade-offs, we start from an existing image classification network. We use a generalized mean layer with exponent p that converts a spatial activation map to a fixed-size vector. The choice of p naturally modulates the trade-off between distinctiveness and invariance [3]. Most importantly, we show that it is an effective way to learn an architecture that can adapt to different resolutions *at test time*. This circumvents the massive engineering and computational effort [25] needed to learn networks for larger input resolutions, which offer higher accuracy [19].

The joint training of classification and instance recognition objectives is based on cross-entropy and contrastive losses, respectively. Remarkably, instance recognition is learned for free, *without using labels specific to instance recognition or image retrieval*: we simply use the identity of the images as labels, and data augmentation as a way to generate different versions of each image.

In summary, our main contributions are as follows:

- We introduce the MultiGrain architecture, which outputs an image embedding incorporating different levels of granularity. Our dual classification+instance objective improves the classification accuracy on its own.
- We show that part of this gain is due to the batching strategy, where each batch contains repeated instances of its images with different data augmentations for the purpose of the retrieval loss;
- We incorporate a pooling layer inspired by image retrieval. It provides a significant boost in classification accuracy when feeding high-resolution images;
- Overall, our architecture offers competing performance both for classification and image retrieval. Noticeably, we report a significant boost in accuracy on Imagenet with a ResNet-50 network over the state of the art.

The paper is organized as follows. Section 2 introduces related works. Section 3 introduces our architecture, the

training procedure and explains how we adapt the resolution at test time. Section 4 reports the main experiments.

2. Related work

Image classification. Most computer vision architectures designed for a wide range of tasks leverage a trunk architecture initially designed for classification, such as Residual networks [18]. An improvement on the trunk architecture eventually translates to better accuracies in other tasks [17], as shown on the detection task of the LSVRC'15 challenge. While recent architectures [23, 24, 48] have exhibited some additional gains, other lines of research have been investigated successfully. For instance, a recent trend [32] is to train high capacity networks by leveraging much larger training sets of weakly annotated data. To our knowledge, the state of the art on Imagenet ILSVRC 2012 benchmark for a model learned from scratch on Imagenet train data only is currently hold by the gigantic AmoebaNet-B architecture [25] (557M parameters), which takes as input 480x480 images.

In our paper, we choose ResNet-50 [18] (25.6M parameters), as this architecture is widely adopted in the literature and many works both on image classification and instance retrieval build upon it.

Image search: from local features to CNN. “Image search” is a generic retrieval task that is usually associated with and evaluated for more specific problems such as landmark recognition [27, 35], particular object recognition [33] or copy detection [8], for which the objective is to find the images most similar to the query in a large image collection. In this paper “image retrieval” will refer to instance-level retrieval, where object instances are as broad as possible. Effective systems for image retrieval rely on accurate image descriptors. Typically, a query image is described by an embedding vector, and the task amounts to searching the nearest neighbors of this vector in the embedding space. Possible improvement include refinement steps such as geometric verification [35], query expansion [4, 44], or database-side pre-processing or augmentation [43, 46].

Local image descriptors are traditionally aggregated to global image descriptors suited for matching in an inverted database, as in the seminal bag-of-words model [41]. After the emergence of convolutional neural networks (CNNs) for large-scale classification on ImageNet [30, 39], it has become apparent that CNNs trained on classification datasets offer very competitive image feature extractors for various vision tasks, including instance retrieval [1, 10, 37].

Specific architectures for particular object retrieval are built upon a regular classification trunk, and modified so the pooling stage gives more spatial locality in order to cope with small objects and clutter. For instance, a competitive baseline for instance retrieval on various datasets is the R-MAC image descriptor [45]. It aggregates regionally pooled features

extracted from a CNN. The authors show that this specialized pooling combined with PCA whitening [26] leads to efficient many-to-many comparisons between image regions, highly beneficial to image retrieval. Gordo et al. [11, 12] show that fine-tuning these regionally-aggregated representations end-to-end on an external image retrieval dataset using a ranking loss yields significant improvements for instance retrieval.

Radenović *et al.* [36] show that R-MAC pooling is advantageously replaced by a generalized mean pooling (see section 3.1), which is a spatial pooling of the features exponentiated to an exponent p over the whole image. The exponentiation localizes the features on the point of interests in the image, replacing regional aggregation in R-MAC.

Multi-task training is an active area of research, motivated by the observation that deep neural networks are transferable to a wide range of vision tasks [37]. Moreover trained deep neural networks exhibit a high level of compressibility [16]. In some cases, sharing the capacity of neural networks between different tasks through shared parameters helps the learning by allowing complementary training among datasets and low-level features. Despite some successes with multi-task networks for vision such as UberNet [29], the design and training of multi-task networks still involve numerous heuristics. Ongoing lines of work include finding the right architecture for an efficient sharing of parameters [38], and finding the right optimization parameters for such networks in order to depart from the traditional setting of single-task single-dataset end-to-end gradient descent, and efficiently weight the gradients in order to obtain a well-performing network in all tasks [14].

Data-augmentation is a cornerstone of the training in large-scale vision applications [30], which improves generalization and reduces over-fitting. In a stochastic gradient descent (SGD) optimization setting, we show that including multiple data-augmented instances of the same image in one optimization batch, rather than having only distinct images in the batch, significantly enhances the effect of data-augmentations and improve the generalization of the network. A related batch augmented (BA) sampling strategy was concurrently introduced by Hoffer et al. [21]. When augmenting the size of the batches in a large-scale distributed optimization of a neural network, they show that filling these bigger batches with data-augmented copies of the image in the batch yields better generalization performance, and uses computing resources more efficiently through reduced data processing time. As discussed in section 3.3 and highlighted in our classification results (section 4.4), we show that a gain in performance under this sampling scheme is obtained *using the same batch size, i.e.*, with a lower number of distinct images per batch. We consider this scheme of repeated augmentations (RA) within the batch as a way to boost the effect of data augmentation over the course of the optimization.

Table 1: Differences between classification and image retrieval. Retrieval architectures incorporate a final pooling layer that is regionalized (RMAC) or magnifies activations (GeM). The triplet loss requires a batching strategy with pairs of matching images.

	classification	retrieval
spatial pooling	avg. pooling	RMAC [44] or GeM [36]
loss	cross-entropy	triplet [11]
batch sampling	diverse	similar images in batch
whitening	no	yes
resolution	“small” (224 ² –300 ²)	large (800–1k×scaled)

Our results indicate that RA is a technique of general interest, beyond large-scale distributed training applications, for improving the generalization of neural networks.

3. Architecture design

Our goal is to develop a convolutional neural network that is suitable for both image classification and instance retrieval. In the current best practices, the architectures and training procedures used for class and instance recognition differ in a significant manner.

This section describes such technical differences, summarized in table 1, together with our solutions to bridge them. This leads us to a unified architecture trainable end-to-end and simultaneously on the two tasks, see fig. 2.

3.1. Spatial pooling operators

This section considers the final spatial pooling layer. Local pooling operators, usually max pooling, are found throughout the layers of most convolutional networks to achieve local invariance to small translations. The spatial pooling converts a 3D activation map produced by a convolutional trunk to a vector.

Classification. In early models such as LeNet-5 [31] or AlexNet [30], the final spatial pooling is just a linearization of the activation map. It is therefore sensitive to the absolute location. Recent architectures such as ResNet and DenseNet employ average pooling, which is permutation invariant and hence offer a more global translation invariance.

Image retrieval requires more localized geometric information: particular objects or landmarks are visually more similar, but the task suffers more from clutter, and a given query image has no specific training data devoted to it. This is why the pooling operator tries to favor more locality. Next we discuss the generalized mean pooling operator.

Let $\mathbf{x} \in \mathbb{R}^{C \times W \times H}$ be the feature tensor computed by a convolutional neural network for a given image, where C is the number of feature channels and H and W are the height and width of the map, respectively. We denote by

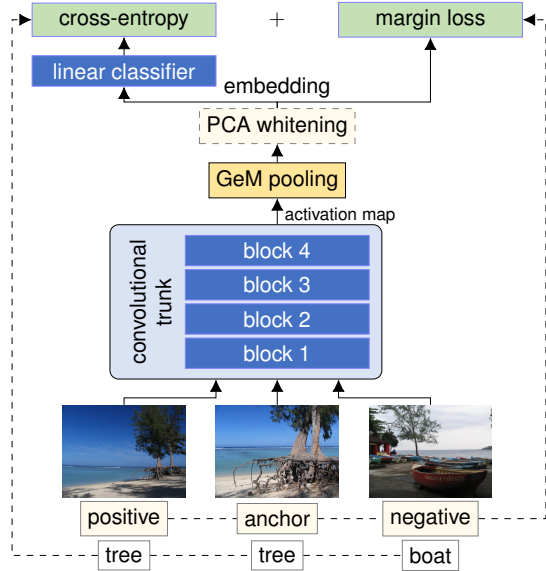


Figure 2: Our Multigrain architecture.

$u \in \Omega = \{1, \dots, H\} \times \{1, \dots, W\}$ a “pixel” in the map, by c the channel, and by x_{cu} the corresponding tensor element: $\mathbf{x} = [x_{cu}]_{c=1..C, u \in \Omega}$. The generalized mean pooling (GeM) layer computes the generalized mean of each channel in a tensor. Formally, the GeM embedding is given by

$$\mathbf{e} = \left[\left(\sum_{u \in \Omega} x_{cu}^p \right)^{\frac{1}{p}} \right]_{c=1..C} \quad (1)$$

where $p > 0$ is a parameter. Setting this exponent as $p > 1$ increases the contrast of the pooled feature map and focus on the salient features of the image [2]. GeM is a generalization of the average pooling commonly used in classification networks ($p = 1$) and of spatial max-pooling layer ($p = \infty$). It is employed in the original R-MAC as an approximation of max pooling [7], yet only recently [36] it was shown to be competitive on its own with R-MAC for image retrieval.

To the best of our knowledge, this paper is the first to apply and evaluate GeM pooling in an image classification setting. More importantly, we show later in this paper that *adjusting the exponent is an effective way to change the input image resolution between train and test time* for all tasks, which explains why image retrieval has benefited from it considering that this task employs higher-resolution images.

3.2. Training objective

In order to combine the classification and retrieval tasks, we use a joint objective function composed of the classification loss and an instance retrieval loss. The two-branch architecture is illustrated in fig. 2 and detailed next.

Classification loss. For classification, we adopt the standard cross-entropy loss. Formally, let $\mathbf{e}_i \in \mathbb{R}^d$ be the embed-

ding computed by the deep network for image i , $\mathbf{w}_c \in \mathbb{R}^d$ the parameters of a linear classifier for class $c \in \{1, \dots, C\}$, and y_i be the ground-truth class for that image. Then

$$\ell^{\text{class}}(\mathbf{e}_i, \mathbf{W}, y_i) = -\langle \mathbf{w}_{y_i}, \mathbf{e}_i \rangle + \log \sum_{c=1}^C \exp \langle \mathbf{w}_c, \mathbf{e}_i \rangle, \quad (2)$$

where $\mathbf{W} = [\mathbf{w}_c]_{c=1..C}$. We omit it for simplicity, but by adding a constant channel to the feature vector, the bias of the classification layer is incorporated in its weight matrix.

Retrieval loss. For image retrieval, embeddings of two matching images (a positive pair) should have distances smaller than embeddings of non-matching images (a negative pair). This is primarily encouraged in two ways. The contrastive loss [15] requires distances between positive pairs to be smaller than a threshold, and distances between negative pairs to be greater. The triplet loss instead requires an image to be closer to a positive sibling than to a negative sibling [40], which is relative property of image triplets.

Implementing these losses requires adjusting multiple parameters, including how pairs and triplets are sampled. These parameters are sometimes hard to tune, especially for the triplet loss.

Wu et al. [47] proposed an effective method that addresses these difficulties. Given a batch of images, they re-normalize their embeddings to the unit sphere, sample negative pairs as a function of the embedding similarity, and use those pairs in a margin loss, a variant of contrastive loss that shares some of the benefits of the triplet loss.

In more detail, given images $i, j \in \mathcal{B}$ in a batch with embeddings $\mathbf{e}_i, \mathbf{e}_j \in \mathbb{R}^d$, the margin loss is expressed as

$$\ell^{\text{retr}}(\mathbf{e}_i, \mathbf{e}_j, \beta, y_{ij}) = \max\{0, \alpha + y_{ij}(D(\mathbf{e}_i, \mathbf{e}_j) - \beta)\} \quad (3)$$

where $D(\mathbf{e}_i, \mathbf{e}_j) = \|\mathbf{e}_i / \|\mathbf{e}_i\| - \mathbf{e}_j / \|\mathbf{e}_j\|\|$ is the Euclidean distance between the normalized embeddings, the label y_{ij} is equal to 1 if the two images match and -1 otherwise, $\alpha > 0$ the margin (a constant hyper-parameter), and $\beta > 0$ is a parameter (learned during training together with the model parameters), controlling the volume of the embedding space occupied embedding vectors. Due to the normalization, $D(\mathbf{e}_i, \mathbf{e}_j)$ is equivalent to a cosine similarity, which, up to whitening (section 3.4), is also used in retrieval.

Loss (3) is computed on a subset of positive and negative pairs $(i, j) \in \mathcal{B}^2$ selected with the sampling [47]

$$\begin{aligned} \mathcal{P}_+(\mathcal{B}) &= \{(i, j) \in \mathcal{B}^2 : y_{ij} = 1\}, \\ \mathcal{P}_-(\mathcal{B}) &= \{(i, j^*) : (i, j) \in \mathcal{P}_+(\mathcal{B}), j^* \sim p(\cdot|i)\}, \\ \mathcal{P}(\mathcal{B}) &= \mathcal{P}_+(\mathcal{B}) \cup \mathcal{P}_-(\mathcal{B}), \end{aligned} \quad (4)$$

where the conditional probability of choosing a negative j for image i is $p(j|i) \propto \min\{\tau, q^{-1}(D(\mathbf{e}_i, \mathbf{e}_j))\} \cdot \mathbf{1}_{\{y_{ij} = -1\}}$, where $\tau > 0$ is a parameter and $q(z) \propto z^{d-2}(1 - z^2/4)^{\frac{d-3}{2}}$ is a PDF that depends on the embedding dimension d .

The use of distance weighted-sampling with margin loss is very suited to our joint training setting: this framework tolerates relatively small batch sizes ($|\mathcal{B}| \sim 80$ to 120 instances) while requiring only a small amount of positives images (3 to 5) of each instance in the batch, without the need for elaborate parameter tuning or offline sampling.

Joint loss and architecture. The joint loss is a combination of classification and retrieval loss weighted by a factor $\lambda \in [0, 1]$. For a batch \mathcal{B} of images, the joint loss writes as

$$\frac{\lambda}{|\mathcal{B}|} \cdot \sum_{i \in \mathcal{B}} \ell^{\text{class}}(e_i, \mathbf{w}, y_i) + \frac{1 - \lambda}{|\mathcal{P}(\mathcal{B})|} \cdot \sum_{(i,j) \in \mathcal{P}(\mathcal{B})} \ell^{\text{retr}}(e_i, e_j, \beta, y_{ij}), \quad (5)$$

i.e., losses are normalized by the number of items in the corresponding summations.

3.3. Training with data-augmented batches

Typical datasets for classification contain several images per object class, but only one image per object instance; instead, typical datasets for instance recognition contain several images per object instance, but no class information. Here, we propose to use only a dataset for image classification and train instance recognition via data augmentation. Applied to any image, data augmentation produces another image that contain the same object instance. This approach does not requires any more supervision than that of standard classification networks.

We introduce a new sampling scheme for training with SGD and data augmentation, which we call *repeated augmentations* (RA). In RA we form an image batch \mathcal{B} by sampling $\lceil |\mathcal{B}|/m \rceil$ different images from the dataset, and transform them up to m times by a set of data augmentations to fill the batch. Thus, the instance level ground-truth $y_{ij} = +1$ iff images i and j are two augmented versions of the same training image.

The key difference with the standard sampling scheme in SGD is that samples are not independent, as augmented versions of the same image are highly correlated [21]. A concern is that this could increase the variance of the noisy gradient estimates in SGD and thus slow down convergence. RA has a surprising behavior. While it does indeed lead to slower performance if the batch size is small, for larger batch sizes RA outperforms the standard i.i.d. scheme – while using the same batch size and learning rate for both schemes. This is different from the observation of [21], which also consider repeated samples in a batch, but simultaneously increases the size of the latter.

We conjecture that the benefit of correlated RA samples is to facilitate learning features that are invariant to the only difference between the repeated images — the augmentations. By comparison, with standard SGD sampling, two versions of the same image are seen only in different epochs. A study

of an idealized problem to further illustrate this phenomenon is given in supplementary A.

3.4. PCA whitening

In order to transfer features learned via data augmentation to standard retrieval datasets, we apply a step of PCA whitening, in accordance with previous works in image retrieval [12, 26]. The Euclidean distance between transformed features is equivalent to the Mahalanobis distance between the input descriptors. This is done after training the network, using an external dataset of unlabelled images.

The effect of PCA whitening can be undone in the parameters of the classification layer, so that the whitened embeddings can be used for both classification and instance retrieval. In detail, let e be an image embedding vector and w_c the weight vector for class c , such that $\langle w_c, e \rangle$ are the outputs of the classifier as in eq. (2). The whitening operation Φ can be written as [12] $\Phi(e) = S \left(\frac{e}{\|e\|} - \mu \right)$ given the whitening matrix S and centering vector μ ; hence

$$\langle w_c, e \rangle = \langle w_c, \Phi^{-1}(\Phi(e)) \rangle = \|e\| (\langle w'_c, \Phi(e) \rangle + b'_c)$$

where $w'_c = S^{-1\top} w_c$ and $b'_c = \langle w_c, \mu \rangle$ are the modified weight and bias for class c . We observed that inducing decorrelation via a loss [5] is insufficient to ensure that features generalize well, which concurs with prior works [12, 36].

3.5. Input sizes

The standard practice in image classification is to resize and center-crop input images to a relatively low resolution, e.g. 224×224 pixels [30], as finer details are often unimportant for classification. The benefits are a smaller memory footprint, faster inference, and possibility of batching the inputs if they are cropped to a common size. On the other hand, image retrieval is typically dependent on finer details in the images, as an instance can be seen under a variety of scales, and cover only a small amount of pixels. Best-performing feature extractors for image retrieval therefore commonly use input sizes of 800 [12] or 1024 [36] pixels for the largest side, without cropping the image. This is impractical for end-to-end training of a joint classification and retrieval network.

Instead, we train our architecture at the standard 224×224 resolution, and use larger input resolutions at test time only. This is possible due to a key advantage of our architecture: a network trained with a pooling exponent p and resolution s can be evaluated at a larger resolution $s^* > s$ using a larger pooling exponent $p^* > p$. This is evidenced in section 4.4.

4. Experiments and Results

After presenting the datasets we work with, we carry out a parametric study (sections 4.2 and 4.3). Then we detail the results we obtain in image classification and retrieval.

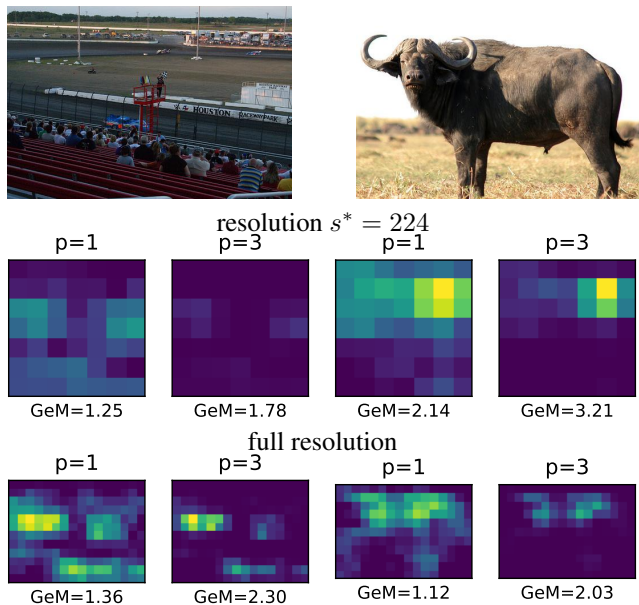


Figure 3: We compare two images, one (difficult) positive for the class “racing car” and one negative. An off-the-shelf ResNet-50 reacts strongly on channel 909 of the last activation map for this class. We show that particular channel when extracted at resolution $s^* = 224$ and at full resolution, with $p^* = 1$ and $p^* = 3$. The color scales are comparable between images for the same resolution and value of p . Below each plot, we indicate the GeM value, ie. component 909 of e (eq. (1)).

4.1. Experimental settings

Base architecture and training settings. The convolutional trunk is ResNet-50 [18]. SGD starts with learning rate 0.1 reduced tenfold at epochs 30, 60, 90 for a total of 120 (a standard setting [34]). The batch size $|\mathcal{B}|$ is set to 512 and an epoch is defined as a fixed number of $T = 5005$ iterations. With uniform batch sampling, one epoch corresponds to two passes over the training set; with repeated augmentations and $m = 3$, one epoch corresponds to $\sim 2/3$ of the images of the training set. All classification baselines are trained using this longer schedule for a fair comparison.

Data augmentation. We use standard flips, random resized crops [22], random lighting noise and a color jittering of brightness, contrast and saturation [30, 22]. We refer to this set of augmentations as “full”. As indicated in table 2 our network reaches 76.2% top-1 validation error under our chosen schedule and data augmentation when trained with cross-entropy alone and uniform batch sampling. This figure is on the high end of accuracies reported for the ResNet-50 network [13, 18] without specially-crafted regularization terms [50] or data augmentations [6].

Pooling exponent. During the end-to-end training of our network, we consider two settings for the pooling exponent in the GeM layer of section 3.1: we set either $p = 1$ or $p = 3$. $p = 1$ corresponds to average pooling, as used in classification architectures. The relevant literature [36] and our preliminary experiments on off-the-shelf classification networks suggest that the value $p = 3$ improves the retrieval performance on standard benchmarks. Figure 3 illustrates this choice. First, it shows that at low resolution, the buffalo reacts stronger on the heat map than the (tiny) car. Changing the p of the GeM does not influence that. At higher resolution, the tiny racing car is detected on the heat map, however the response is still relatively strong over many pixels of the buffalo image. When applying the GeM with $p = 3$, the spurious detections on the buffalo image are reduced, while the car is detected with high confidence.

Input size and cropping. As described in section 3.5, we train our network on crops of size 224×224 pixels. For testing, we experiment with computing MultiGrain embeddings at resolutions $s^* = 224, 500, 800$. For resolution $s^* = 224$, we follow the classical image classification protocol “resolution 224”: the smallest side of an image is resized to 256 and then a 224×224 central crop is extracted. For resolution $s^* > 224$, we instead follow the protocol common in image retrieval and resize the largest side of the image to the desired number of pixels and evaluate the network on the rectangular image, without cropping.

Margin loss and batch sampling. We use $m = 3$ data-augmented repetitions per batch. We use the default margin loss hyperparameters of [47] (details in supplementary B). As in [47] the distance-weighted sampling is performed independently on each of the 4 GPUs used for training.

Datasets. We train our networks on the ImageNet-2012 training set of 1.2 million images labelled into 1,000 object categories [39]. Classification accuracies are reported on the 50,000 validation images of this dataset. Regarding image retrieval, we report the mean average precision on the INRIA Holidays dataset [27], with images rotated manually when necessary, as in prior work evaluations of this dataset [11]. We also report the accuracy on the University of Kentucky (UKB) object recognition benchmark [33], which contains 2,550 instances of objects under 4 varying viewpoints each; each image is used as a query to find its 4 closest neighbours in embedding space; the number of correct neighbours is averaged across all images, yielding a performance measure between 1 and 4. We also report the performance of our network in a copy detection setting, indicating the mean average precision on the “strong” subset of the INRIA Copydays dataset [8]. We add 10K distractor images randomly sampled from the YFCC100M large-scale collection of unlabelled images [42]. We call the combination C10k.

The PCA whitening transformations are computed from

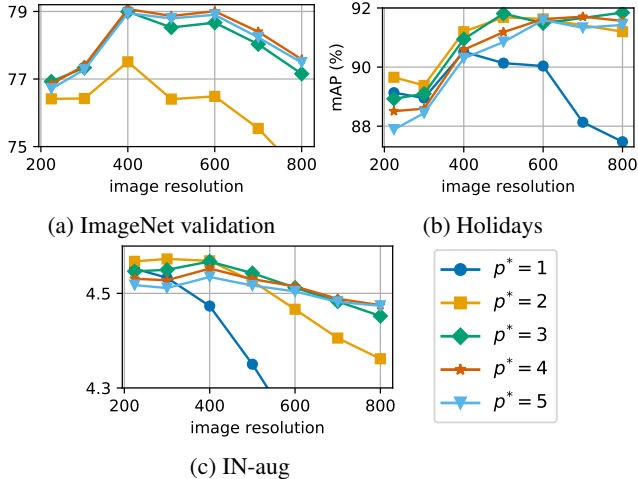


Figure 4: Retrieval and classification accuracies as a function of pooling exponent p^* and the image resolution. At training time, the pooling was $p = 3$.

the features of 20K images from YFCC100M, distinct from the C10k distractors.

4.2. Expanding resolution with pooling exponent

A baseline experiment is to train using our training schedule with repeated augmentation sampling and pooling exponent $p = 3$; as seen in table 2, this leads to a 76.9% top-1 validation accuracy, 0.7 points above the non-RA baseline.

Then, we use the network as a feature extractor for images at resolutions $s^* > 224$ (used at training time) and vary the exponents $p^* \neq p = 3$ at test time.

Figures 4a and 4b show the classification accuracy on ImageNet validation and the retrieval accuracy on Holidays at different resolutions, for different values of the test pooling exponent p^* . As expected, at $s^* = 224$, the pooling exponent yielding best accuracy in classification is the exponent with which the network has been trained, $p^* = 3$. We find that in general evaluating at larger scale requires choosing an exponent $p^* > p$, both for classification and for retrieval.

For the next experiment, we create a synthetic retrieval dataset **IN-aug** by picking 2,000 images from the training set of ImageNet, 2 per class, and creating 5 augmented copies of each of them, using the ‘full’ data augmentation described before. We evaluate the retrieval accuracy on IN-aug in a fashion similar to UKBench, with an accuracy ranging from 1 to 5. We see from fig. 4c that the optimal p^* on IN-aug behaves similarly as the best p^* on the Holidays retrieval dataset. In the following, we therefore pick the best-performing $p^* \in \{1, 2, \dots, 10\}$ on IN-aug; for the $p = 3$, $\lambda = 0.5$ experiment, this corresponds to

s^*	224	500	800
p^*	3	4	5

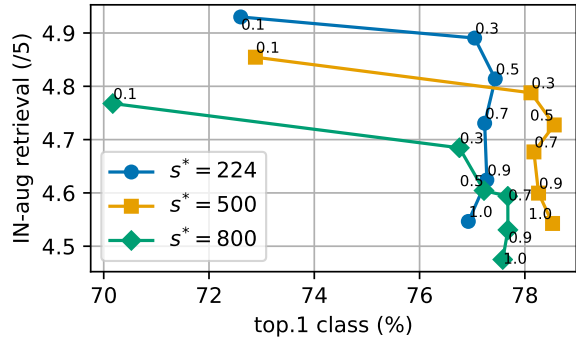


Figure 5: Retrieval accuracy on IN-aug vs. classification performance for the $p = 3$ MultiGrain network trained at resolution 224^2 . The indicated numbers correspond to the weight λ which we vary in order to sweep over the tradeoffs.

4.3. Impact of the tradeoff parameter

We experiment with varying tradeoff parameters λ among $\{0.1, 0.3, 0.5, 0.7, 0.9, 1.0\}$. Figure 5 shows the tradeoff on IN-aug. At $\lambda = 0.1$ we get the best performance on the surrogate retrieval task but low classification performance. With cross-entropy and repeated augmentations alone ($\lambda = 1$), the classification performance is good (76.9% at $s^* = 224$) but retrieval performance low. Interestingly, for the intermediate $\lambda = 0.5$, we see a higher classification performance (77.4% at $s^* = 224$) than for $\lambda = 1$. Thus, the margin loss leads to a performance gain both for the surrogate retrieval task and for the classification task.

We set $\lambda = 0.5$ in our following experiments, as it corresponds to the best classification accuracy at resolutions $s^* = 224$ and 500 pixels.

4.4. Classification results

From now on, our MultiGrain nets are trained at resolution $s = 224$ with exponent $p = 1$ (standard average pooling) or $p = 3$ in the GeM pooling. For each evaluation resolutions $s^* = 224, 500, 800$, the same exponent p^* is selected according to section 4.2, yielding a single embedding for classification and for the retrieval.

Table 2 presents the classification results. There is a large improvement in classification performance from our baseline Resnet-50 with $p = 1$, $s = 224$, ‘full’ data augmentation (76.2% top-1 accuracy), to a MultiGrain model at $p = 3$, $\lambda = 0.5$, $s = 500$ (78.6% top-1). We identify four sources for this improvement:

1. Repeated augmentations: adding RA batch sampling (section 3.3) yields an improvement of +0.6% ($p = 1$).
2. Margin loss: the retrieval loss helps the generalizing effect of data augmentation: +0.2% ($p = 1$).
3. $p = 3$ pooling: GeM at training (section 3.1) allows the

Table 2: ImageNet 2012 validation performance given as top-1 / top-5 accuracies (%). Resnet-50 is a single-head classification baseline trained with our training schedule, data augmentation, and uniform batch sampling. MultiGrain uses the same Resnet-50 trunk. At resolutions $s^* > 224$ we evaluate with exponent p^* as described in section 4.2.

Architecture	λ	data aug.	scale s^*	train-time pooling	
				$p = 1$	$p = 3$
ResNet-50		full	224	76.2 / 92.9	76.2 / 93.1
MultiGrain	1	full	224	76.8 / 93.2	76.9 / 93.5
MultiGrain	0.5	full	224	77.0 / 93.6	77.4 / 93.6
MultiGrain	0.5	AA	224	77.4 / 93.6	78.2 / 93.9
MultiGrain	0.5	full	500	76.5 / 93.5	78.6 / 94.4
MultiGrain	0.5	AA	500	77.7 / 94.0	79.4 / 94.8
MultiGrain	0.5	full	800	73.5 / 93.5	77.2 / 93.5
MultiGrain	0.5	AA	800	74.1 / 91.8	77.8 / 93.9
PyTorch model zoo			224	76.1 / 92.9	
mixup [50]			224	76.7 / 94.4	
BA ($ \mathcal{B} = 1024$) [21]			224	76.9 / -	
AutoAugment [6]			224	77.6 / 93.8	

margin loss to have a much stronger effect thanks to increased localization of the features: +0.4%.

- Expanding resolution: evaluating at resolution 500 adds +1.2% to the $p = 3$ MultiGrain network, reaching the 78.6 top-1 accuracy. This is made possible by the $p = 3$ training – which yields sparser features, more generalizable over different resolutions, and by the p^* pooling adaptation – without it the performance at this resolution is only 78.0%.

The p^* selection for evaluation at higher resolutions has its limits: at 800 pixels, due to the large discrepancy between the training and testing scale for the feature extractor, the accuracy goes down to 77.2% (which would be 76.2% without the p^* adaptation).

AutoAugment. To show that our findings generalize beyond our particular choice of data-augmentation, we experiment with AutoAugment [6] (AA) generated augmentations. These augmentations were selected using reinforcement learning techniques to improve the accuracy of classification networks on ImageNet. We do not do this reinforcement learning search, but directly implement the published data-augmentations strategy found by the algorithm. [6] train their Resnet-50 model using a long schedule of 270 passes over the dataset, with batch size 4096. We have observed that this longer training gives more impact to the AA-generated augmentations. We therefore use a longer schedule of 7508 iterations per epoch, keeping the batch size $|\mathcal{B}| = 512$.

We find that our observations generalize to this data-augmentation. MultiGrain reaches 78.2% top-1 accuracy

at resolution 224 with $p = 3, \lambda = 0.5$. To the best of our knowledge, this is the best top-1 accuracy reported for Resnet-50 when training and evaluating at this resolution, significantly higher than the 77.6% reported with AutoAugment alone [6] or 76.7% for mixup [50]. Using a higher resolution at test-time improves the accuracy further: we obtain 79.4% top-1 accuracy at resolution 500. Our strategy of adapting the pooling exponent to larger resolution is effective, and significantly outperforms the state of the art performance for a ResNet-50 learned on ImageNet at training resolution 224.

4.5. Retrieval results

We turn to our retrieval results in in table 3. We see that our MultiGrain nets have improved accuracies on the three datasets with respect to our baseline Resnet-50. Repeated augmentations (RA) is a key ingredient here.

We compare with baselines where no annotated retrieval dataset is used. [11, 12] give off-the-shelf network accuracies with R-MAC pooling. MultiGrain compares favorably with their results at a comparable resolution ($s^* = 800$). They reach accuracies above 93% mAP on Holidays but this requires a resolution $s \geq 1000$ pixels; moreover R-MAC, having no obvious extension to a classification setting, does not yield a single embedding for classification and retrieval.

It is also worth noting that we reach reasonable retrieval performance at resolution $s^* = 500$, which is a interesting operating point with respect to the traditional inference resolutions $s = 800-1000$ for retrieval. Indeed, a forward pass of Resnet-50 on 16 processor cores takes 3.80s at resolution 500, against 18.9s at resolution 1024 ($5\times$ slower). Because of this quadratic increase in timing, and the single embedding computed by MultiGrain, our solution is particularly adapted to large-scale or low-resource vision applications.

For comparison, we also report some older related results on the UKB and C10k datasets, that are not competitive with MultiGrain. Neural codes [1] is one of the first works on retrieval with deep features. The Fisher vector[28] is a pooling method that uses local SIFT descriptors.

Parameters. At resolutions 224, 500 we see that the results when adding margin loss ($\lambda = 0.5$) are slightly lower than without ($\lambda = 1$). Part of this is due to the limited transfer from the IN-aug task to the variations observed in retrieval datasets. However, other choices of λ could also improve the effect of margin loss. Note that the AA augmentations do not transfer as well to the retrieval task, which can be explained by their specificity to Imagenet classification.

A particular dataset could also be targetted by searching for data-transformations particularly suited to this dataset; this is not the aim of our present study, where a single embedding for classification and retrieval datasets is desired.

Using clustering techniques, [36] generates an automatically annotated retrieval dataset with which they fine-tune

Table 3: Instance search and copy detection results, on Holidays (% mAP), UKB (/4), Copydays + 10k distractors (CD10k, % mAP). We use $p = 3$ pooling at training for our MultiGrain models. At larger test-time resolution we use p^* as described in section 4.2, same as in table 2.

Method	λ	$s^* =$	Holidays			UKB			CD10k		
			224	500	800	224	500	800	224	500	800
PyTorch model zoo			85.5	86.6	82.8	3.71	3.85	3.80	61.5	61.1	43.0
ResNet-50 ($p = 1$)			83.5	88.8	87.1	3.60	3.79	3.82	59.2	69.9	66.2
ResNet-50 ($p = 3$)			86.8	90.0	90.4	3.73	3.87	3.89	70.6	78.9	75.7
MultiGrain	1		88.9	91.8	91.6	3.78	3.89	3.91	75.1	81.2	82.5
MultiGrain	0.5		88.3	91.5	92.5	3.78	3.90	3.91	74.1	80.7	78.6
MultiGrain + AA	0.5		86.5	90.3	89.4	3.75	3.89	3.90	69.7	77.8	76.1
ResNet-50 RMAC, $s = 724$ [11]					90.9						
ResNet-50 RMAC, $s = 1024$ [11]					93.3						
ResNet-101 RMAC, $s = 800$ [12]					91.4		3.89				
GeM, $s = 1000$ [43]					93.9						
Neural codes [1]			79.3			3.56					
Fisher vectors [28]					63.4		3.35			42.7	

their network. This fine-tuning is likely to lead to a drop in accuracy of the embeddings for classification through catastrophic forgetting [9, 20], and therefore again does not lead to a unified embedding.

5. Conclusion

MultiGrain is a unified embedding for image classification and instance retrieval. It relies on a classical convolutional neural network trunk, with a GeM layer topped with two heads at training time. We discovered that by adjusting this pooling layer, we are able to increase the resolution of images used at inference time, while maintaining a small resolution at training time. We show that MultiGrain embeddings can perform well on classification and retrieval. More surprisingly, MultiGrain also sets a new state of the art on pure classification compared to all results obtained with the same convolutional trunk.

This is another indication that retrieval and classification are two interlinked tasks, and advances in one field benefit to the other. In the future, we plan to measure the behavior of MultiGrain on fine-grained classification, where the gap between the two tasks is even more narrow.

Acknowledgments. We thank Kaiming He for useful feedback and references. Maxim Berman is supported by Research Foundation - Flanders (FWO) through project number GOA2716N. PSI-ESAT acknowledges a GPU server donation from FAIR Partnership Program.

References

- [1] A. Babenko, A. Slesarev, A. Chigorin, and V. Lempitsky. Neural codes for image retrieval. In *Proc. ECCV*, pages 584–599. Springer, 2014. [2](#), [8](#), [9](#)
- [2] L. Bo and C. Sminchisescu. Efficient match kernel between sets of features for visual recognition. In *Proc. NIPS*, 2009. [4](#)
- [3] Y.-L. Boureau, J. Ponce, and Y. LeCun. A theoretical analysis of feature pooling in visual recognition. In *Proc. ICML*, 2010. [2](#)
- [4] O. Chum, J. Philbin, J. Sivic, M. Isard, and A. Zisserman. Total recall: Automatic query expansion with a generative feature model for object retrieval. In *Proc. ICCV*, 2007. [2](#)
- [5] M. Cogswell, F. Ahmed, R. B. Girshick, C. L. Zitnick, and D. Batra. Reducing overfitting in deep networks by decorrelating representations. *CoRR*, abs/1511.06068, 2016. [5](#)
- [6] E. D. Cubuk, B. Zoph, D. Mane, V. Vasudevan, and Q. V. Le. Autoaugment: Learning augmentation policies from data. *arXiv preprint arXiv:1805.09501*, 2018. [6](#), [8](#)
- [7] P. Dollár, Z. Tu, P. Perona, and S. Belongie. Integral channel features. In *Proc. BMVC*, 2009. [4](#)
- [8] M. Douze, H. Jégou, H. Sandhwalia, L. Amsaleg, and C. Schmid. Evaluation of gist descriptors for web-scale image search. In *Proc. CIVR*, 2009. [2](#), [6](#)
- [9] R. M. French. Catastrophic forgetting in connectionist networks. *Trends in Cognitive Sciences*, 3:128–135, 1999. [9](#)
- [10] Y. Gong, L. Wang, R. Guo, and S. Lazebnik. Multi-scale orderless pooling of deep convolutional activation features. In *Proc. ECCV*, pages 392–407. Springer, 2014. [2](#)
- [11] A. Gordo, J. Almazán, J. Revaud, and D. Larlus. Deep image retrieval: Learning global representations for image search. In *Proc. ECCV*, 2016. [3](#), [6](#), [8](#), [9](#)
- [12] A. Gordo, J. Almazán, J. Revaud, and D. Larlus. End-to-end learning of deep visual representations for image retrieval. *IJCV*, 124:237–254, 2017. [3](#), [5](#), [8](#), [9](#)
- [13] P. Goyal, P. Dollár, R. Girshick, P. Noordhuis, L. Wesolowski, A. Kyrola, A. Tulloch, Y. Jia, and K. He. Accurate, large minibatch sgd: training imagenet in 1 hour. *arXiv preprint arXiv:1706.02677*, 2017. [6](#)
- [14] M. Guo, A. Haque, D.-A. Huang, S. Yeung, and L. Fei-Fei. Dynamic task prioritization for multitask learning. In *Proc. ECCV*, pages 282–299. Springer, 2018. [3](#)
- [15] R. Hadsell, S. Chopra, and Y. LeCun. Dimensionality reduction by learning an invariant mapping. In *Proc. CVPR*, 2006. [4](#)
- [16] S. Han, H. Mao, and W. J. Dally. Deep compression: Compressing deep neural networks with pruning, trained quantization and Huffman coding. *arXiv preprint arXiv:1510.00149*, 2015. [3](#)
- [17] K. He, G. Gkioxari, P. Dollár, and R. Girshick. Mask r-cnn. In *Proc. ICCV*, 2017. [2](#)
- [18] K. He, X. Zhang, S. Ren, and J. Sun. Deep residual learning for image recognition. In *Proc. CVPR*, 2016. [2](#), [6](#)
- [19] K. He, X. Zhang, S. Ren, and J. Sun. Identity mappings in deep residual networks. In *Proc. ECCV*, 2016. [2](#)
- [20] G. E. Hinton and R. Salakhutdinov. Reducing the dimensionality of data with neural networks. *Science*, 313 5786:504–7, 2006. [9](#)
- [21] E. Hoffer, T. Ben-Nun, I. Hubara, N. Giladi, T. Hoefler, and D. Soudry. Augment your batch: better training with larger batches. *arXiv e-prints*, page arXiv:1901.09335, Jan. 2019. [3](#), [5](#), [8](#)
- [22] A. G. Howard. Some improvements on deep convolutional neural network based image classification. *arXiv preprint arXiv:1312.5402*, 2013. [6](#)
- [23] J. Hu, L. Shen, and G. Sun. Squeeze-and-excitation networks. In *Proc. CVPR*, 2018. [2](#)
- [24] G. Huang, Z. Liu, L. Van Der Maaten, and K. Q. Weinberger. Densely connected convolutional networks. In *Proc. CVPR*, 2017. [2](#)
- [25] Y. Huang, Y. Cheng, D. Chen, H. Lee, J. Ngiam, Q. V. Le, and Z. Chen. Gpipe: Efficient training of giant neural networks using pipeline parallelism. *arXiv preprint arXiv:1811.06965*, 2018. [2](#)
- [26] H. Jégou and O. Chum. Negative evidences and co-occurrences in image retrieval: The benefit of pca and whitening. In *Proc. ECCV*, pages 774–787. Springer, 2012. [3](#), [5](#)
- [27] H. Jégou, M. Douze, and C. Schmid. Hamming embedding and weak geometric consistency for large scale image search. In *Proc. ECCV*, 2008. [2](#), [6](#)
- [28] H. Jégou, F. Perronnin, M. Douze, J. Sánchez, P. Perez, and C. Schmid. Aggregating local image descriptors into compact codes. *PAMI*, 34(9), 2012. [8](#), [9](#)
- [29] I. Kokkinos. Ubernet: Training a universal convolutional neural network for low-, mid-, and high-level vision using diverse datasets and limited memory. *Proc. CVPR*, pages 5454–5463, 2017. [2](#), [3](#)
- [30] A. Krizhevsky, I. Sutskever, and G. E. Hinton. Imagenet classification with deep convolutional neural networks. In *Proc. NIPS*, pages 1097–1105, 2012. [2](#), [3](#), [5](#), [6](#)
- [31] Y. LeCun, B. Boser, J. S. Denker, D. Henderson, R. E. Howard, W. Hubbard, and L. D. Jackel. Backpropagation applied to handwritten zip code recognition. *Neural computation*, 1(4):541–551, 1989. [3](#)
- [32] D. Mahajan, R. Girshick, V. Ramanathan, K. He, M. Paluri, Y. Li, A. Bharambe, and L. van der Maaten. Exploring the limits of weakly supervised pretraining. *arXiv preprint arXiv:1805.00932*, 2018. [2](#)
- [33] D. Nister and H. Stewenius. Scalable recognition with a vocabulary tree. In *Proc. CVPR*, 2006. [2](#), [6](#)
- [34] A. Paszke, S. Gross, S. Chintala, G. Chanan, E. Yang, Z. DeVito, Z. Lin, A. Desmaison, L. Antiga, and A. Lerer. Automatic differentiation in pytorch. In *NIPS Autodiff Workshop*, 2017. [6](#)
- [35] J. Philbin, O. Chum, M. Isard, J. Sivic, and A. Zisserman. Object retrieval with large vocabularies and fast spatial matching. In *Proc. CVPR*, 2007. [2](#)
- [36] F. Radenović, G. Tolias, and O. Chum. Fine-tuning cnn image retrieval with no human annotation. *TPAMI*, 2018. [3](#), [4](#), [5](#), [6](#), [8](#)
- [37] A. S. Razavian, H. Azizpour, J. Sullivan, and S. Carlsson. Cnn features off-the-shelf: An astounding baseline for recognition. *Proc. CVPR Workshop*, pages 512–519, 2014. [2](#), [3](#)
- [38] S.-A. Rebuffi, H. Bilen, and A. Vedaldi. Efficient parametrization of multi-domain deep neural networks. In *Proc. CVPR*, pages 8119–8127, 2018. [3](#)

- [39] O. Russakovsky, J. Deng, H. Su, J. Krause, S. Satheesh, S. Ma, Z. Huang, A. Karpathy, A. Khosla, M. Bernstein, A. C. Berg, and L. Fei-Fei. ImageNet Large Scale Visual Recognition Challenge. *IJCV*, 115(3):211–252, 2015. 2, 6
- [40] F. Schroff, D. Kalenichenko, and J. Philbin. Facenet: A unified embedding for face recognition and clustering. In *Proc. CVPR*, pages 815–823, 2015. 4
- [41] J. Sivic and A. Zisserman. Video google: A text retrieval approach to object matching in videos. In *Proc. ICCV*, 2003. 2
- [42] B. Thomee, D. A. Shamma, G. Friedland, B. Elizalde, K. Ni, D. Poland, D. Borth, and L.-J. Li. Yfcc100m: the new data in multimedia research. *Commun. ACM*, 59:64–73, 2016. 6
- [43] G. Tolias, Y. Avrithis, and H. Jégou. Image search with selective match kernels: aggregation across single and multiple images. *IJCV*, 116(3):247–261, 2016. 2, 9
- [44] G. Tolias and H. Jégou. Visual query expansion with or without geometry: Refining local descriptors by feature aggregation. *Pattern Recognition*, 47(10):3466 – 3476, 2014. 2, 3
- [45] G. Tolias, R. Sicre, and H. Jégou. Particular object retrieval with integral max-pooling of cnn activations. *CoRR*, abs/1511.05879, 2015. 2
- [46] P. Turcot and D. G. Lowe. Better matching with fewer features: The selection of useful features in large database recognition problems. In *Proc. ICCV*, 2009. 2
- [47] C.-Y. Wu, R. Manmatha, A. J. Smola, and P. Krähenbühl. Sampling matters in deep embedding learning. In *Proc. ICCV*, 2017. 4, 6
- [48] S. Xie, R. B. Girshick, P. Dollár, Z. Tu, and K. He. Aggregated residual transformations for deep neural networks. *Proc. CVPR*, pages 5987–5995, 2017. 2
- [49] A. R. Zamir, A. Sax, W. B. Shen, L. J. Guibas, J. Malik, and S. Savarese. Taskonomy: Disentangling task transfer learning. *Proc. CVPR*, pages 3712–3722, 2018. 2
- [50] H. Zhang, M. Cisse, Y. N. Dauphin, and D. Lopez-Paz. mixup: Beyond empirical risk minimization. In *Proc. ICLR*, 2018. 6, 8

MultiGrain: a unified image embedding for classes and instances

Supplementary Material

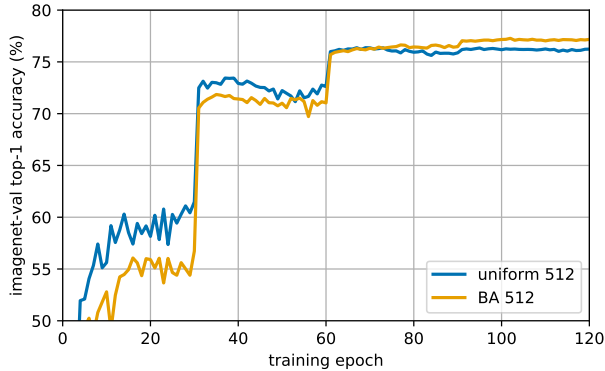


Figure A.1: Evolution of the validation accuracy on ImageNet-val with and without data-augmented batches.

A. Data-augmented batches: toy model

We have observed in Sections 3.3 and 4.3 that training our architecture (ResNet-50 trunk) with data-augmented batches yields improvements with respect to the vanilla uniform sampling scheme, despite the decrease in single image diversity.

This observation holds even in the absence of ranking triplet loss, all things being equal otherwise: same number of iterations per epoch, number of epochs, learning rate schedule, and batch size. As an example, fig. A.1 shows the evolution of the validation accuracy of our network trained under cross-entropy with our training schedule and a $p = 1$ pooling, batches of size 512, with the data augmentation introduced in section 4.1, with uniform batches vs. with batch sampling. While initial epochs suffer from the reduced diversity of the batches compared to the uniformly-sampled variant, the reinforced effect on data augmentation compensates for this in the long run, and makes the batch-augmented variant reach a higher final accuracy.

Since we observe this better performance even for a pure image classification task, an interesting question is whether this benefit is specific to our architecture and training method (batch-norm, etc), or if it is more generally applicable? Hereafter we validate the second hypothesis by an analysis on a linear model and synthetic classification task.

We consider an idealized model of the effect of including different data-augmented instances of the same image in one

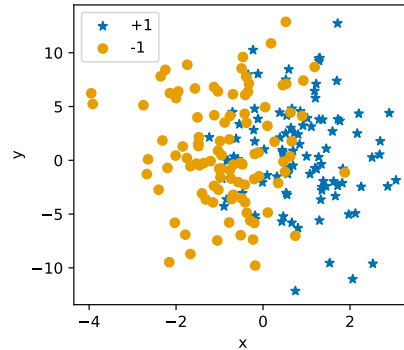


Figure A.2: Training set for the toy model in appendix A.

batch using standard stochastic gradient descent. We create a synthetic training set \mathcal{D} of points pictured in fig. A.2 of $N = 100$ positive and $N = 100$ negative training points $\mathbf{p}^i = (p_x^i, p_y^i)$ by sampling from two shifted 2D Gaussian distribution

$$\begin{aligned} p_x^i &\sim \mathcal{N}(\mu = 0, \sigma = 5) \\ p_y^i &\sim \mathcal{N}(\mu = y_i^*, \sigma = 1) \end{aligned} \quad (\text{A.1})$$

with $y_i^* = \pm 1$ the ground truth label. We sample a test dataset in the same manner.

We consider the SGD training of an SVM

$$f_{\mathbf{w}}(\mathbf{p}_i) = \mathbf{w}^\top \mathbf{p}_i \quad (\text{A.2})$$

using the Hinge loss

$$\ell^{\text{hinge}} = \max(1 - y_i^* f_{\mathbf{w}}(\mathbf{p}_i), 0). \quad (\text{A.3})$$

We consider the symmetry across the x-axis

$$\phi((p_x^i, p_y^i)) = \phi((p_x^i, -p_y^i)) \quad (\text{A.4})$$

as a label-preserving data-augmentation suited to our synthetic dataset. We train the SVM (A.2) using one pass through the data-augmented dataset $\tilde{\mathcal{D}}$ of size $4N$, using batches of size 2.

The only difference between the two optimization schedules is the order in which the samples are batched and presented to the network. We consider two batch sampling strategies:

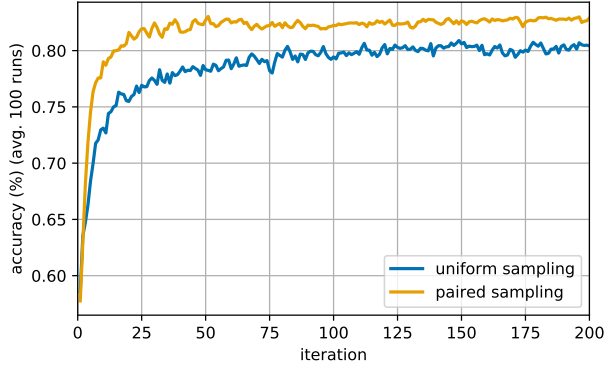


Figure A.3: Evolution of the test accuracy of the SVM of the toy model data, averaged across 100 runs.

- We sample the elements of the batch randomly from $\bar{\mathcal{D}}$, without replacement;
- We generate a batch by pairing a random element from $\bar{\mathcal{D}}$ and its data-augmentation, removing these two elements from $\bar{\mathcal{D}}$.

Figure A.3 shows the evaluation of the accuracy with the iterations in both of these cases, averaged across 100 runs. It is clear that pairing the data-augmented pairs in one batch accelerates the convergence of this model. This idealized experiments demonstrates that there are cases in which the repeated augmentation scheme provides an optimization and generalization boost, and reinforces the effect of data augmentation.

B. Margin loss parameters

Table B.1: Training hyper-parameters

parameter	value
margin α	0.2
initial β_0	1.2
β learning rate	0.1

Table B.1 gives the value of the hyper-parameters for the margin loss used during the training of our models.

C. Parameters of the “full” data-augmentation

Table C.1 gives the transformations in the “full” data augmentation used in our experiments (section 4.1), along with their parameters.

Table C.1: “full” data-augmentation: transformations and parameters

transformation	parameter range
horizontal flip	
random resized crop	scale $\in [0.08, 1.0]$ ratio $\in [3/4, 4/3]$
color jitter	brightness 0.3 contrast 0.3 saturation 0.3
lighting transform	intensity 0.1